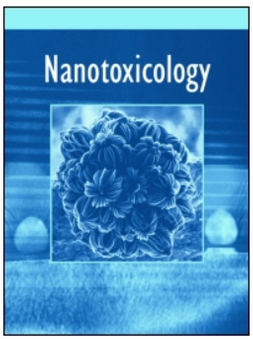

Nanotoxicology

ISSN: 1743-5390 (Print) 1743-5404 (Online) Journal homepage: http://www.tandfonline.com/loi/inan20

Compared in vivo toxicity in mice of lung delivered biodegradable and non-biodegradable nanoparticles

Letícia Aragao-Santiago, Hervé Hillaireau, Nadège Grabowski, Simona Mura, Thais L. Nascimento, Sandrine Dufort, Jean-Luc Coll, Nicolas Tsapis & Elias Fattal

To cite this article: Letícia Aragao-Santiago, Hervé Hillaireau, Nadège Grabowski, Simona Mura, Thais L. Nascimento, Sandrine Dufort, Jean-Luc Coll, Nicolas Tsapis & Elias Fattal (2015): Compared in vivo toxicity in mice of lung delivered biodegradable and non-biodegradable nanoparticles, Nanotoxicology, DOI: 10.3109/17435390.2015.1054908

To link to this article: http://dx.doi.org/10.3109/17435390.2015.1054908

Published online: 17 Nov 2015.

http://informahealthcare.com/nan
ISSN: 1743-5390 (print), 1743-5404 (electronic)

Nanotoxicology

Nanotoxicology, Early Online: 1–11
 DOI: 10.3109/17435390.2015.1054908

Taylor & Francis
Taylor & Francis Group

ORIGINAL ARTICLE

Compared *in vivo* toxicity in mice of lung delivered biodegradable and non-biodegradable nanoparticles

Letícia Aragao-Santiago[1,2], Hervé Hillaireau[1,2], Nadège Grabowski[1,2], Simona Mura[1,2], Thais L. Nascimento[1,2], Sandrine Dufort[3,4], Jean-Luc Coll[3,4], Nicolas Tsapis[1,2], and Elias Fattal[1,2]

[1]*Faculté de Pharmacie, Institut Galien Paris-Sud, LabEx LERMIT, Université Paris-Sud, Chatenay-Malabry Cedex, France,* [2]*CNRS, UMR 8612, Chatenay-Malabry Cedex, France,* [3]*INSERM U823, Institut Albert Bonniot, Grenoble, France, and* [4]*Université Joseph Fourier, Grenoble, France*

Abstract

To design nanoparticle (NP)-based drug delivery systems for pulmonary administration, biodegradable materials are considered safe, but their potential toxicity is poorly explored. We here explore the lung toxicity in mice of biodegradable nanoparticles (NPs) and compare it to the toxicity of non-biodegradable ones. NP formulations of poly(D,L-lactide-*co*-glycolide) (PLGA) coated with chitosan (CS), poloxamer 188 (PF68) or poly(vinyl alcohol) (PVA), which renders 200 nm NPs of positive, negative or neutral surface charge respectively, were analyzed for their biodistribution by *in vivo* fluorescence imaging and their inflammatory potential after single lung nebulization in mice. After exposure, analysis of bronchoalveolar lavage (BAL) cell population, protein secretion and cytokine release as well as lung histology were carried out. The inflammatory response was compared to the one induced by non-biodegradable counterparts, namely, TiO_2 of rutile and anatase crystal form and polystyrene (PS). PLGA NPs were mostly present in mice lungs, with little passage to other organs. An increase in neutrophil recruitment was observed in mice exposed to PS NPs 24 h after nebulization, which declined at 48 h. This result was supported by an increase in interleukin (IL)-6 and tumor necrosis factor α (TNFα) in BAL supernatant at 24 h. TiO_2 anatase NPs were still present in lung cells 48 h after nebulization and induced the expression of pro-inflammatory cytokines and the recruitment of polymorphonuclear cells to BAL. In contrast, regardless of their surface charge, PLGA NPs did not induce significant changes in the inflammation markers analyzed. In conclusion, these results point out to a safe use of PLGA NPs regardless of their surface coating compared to non-biodegradable ones.

Keywords

Biodegradable, inflammation, lung, nanoparticle

History

Received 19 October 2014
Revised 11 May 2015
Accepted 18 May 2015
Published online 12 November 2015

Introduction

Lung administration represents a non-invasive route that can be used for local or systemic drug delivery thanks to the high absorption surface, weak enzymatic activity, high blood supply of the pulmonary region and avoidance of first-pass metabolism, providing a faster therapeutic action (Mansour et al., 2009). A large range of biodegradable nanocarriers can be considered for such an administration. Among them, poly(lactide-co-glycolide) (PLGA)-based nanaoparticles (NPs) present a high interest for drug delivery for their biocompatibility and complete degradability (Panyam & Labhasetwar, 2003). In addition, NPs made of such co-polymer can easily be surface-modified for an efficient targeting and several different drugs have been loaded onto these particles, from small molecules to macromolecules (Fattal & Tsapis, 2014).

Compared to bulk materials, NPs show unique characteristics such as their minute size, higher specific surface area and surface chemical characteristic and reactivity. However, these well-defined characteristics have raised concern with regards to their safety and toxicity (Oberdorster et al., 2005). Although biodegradable NPs could be assumed safe due to their biodegradability, their nano characteristics as well as byproducts of their degradation could pose a health risk, making indispensable the need to assess their safety (Singh & Ramarao, 2013).

Our group has developed PLGA NPs with different surface properties with the aim of designing a drug delivery vector for lung diseases (Grabowski et al., 2013; Mura et al., 2011b). By means of addition of three different stabilizing agents – chitosan (CS), poly(vinyl alcohol) (PVA) or poloxamer 188 (Pluronic® F68, PF68), PLGA NPs were obtained that displayed a positive, neutral or negative surface charge, respectively. In a recent study, a mild inflammatory response to stabilized NPs was detected *in vitro* on a co-culture of lung epithelial cells and macrophage-like cells (Grabowski et al., 2013, 2014). This study completes the previous ones and investigates the *in vivo* biodistribution and toxicity of these biodegradable PLGA NPs displaying different surface properties, and compares them to non-biodegradable counterparts, either inorganic such as TiO_2 of rutile and anatase crystal form, or polymeric such as polystyrene (PS).

Methods

Nanoparticle preparation

PLGA NPs were prepared by the emulsion/evaporation method, as previously described by Grabowski et al. (2013) to render

Correspondence: Hervé Hillaireau, Faculté de Pharmacie, Institut Galien Paris-Sud, Université de Paris-Sud 11, UMR CNRS 8612, 5 rue JB Clément, 92296 Chatenay-Malabry Cedex, France. Tel: +33 1 46 83 54 27. Fax: +33 1 46 61 93 34. E-mail: herve.hillaireau@u-psud.fr

particles with a neutral, positive or negative surface charge. Neutral (PLGA/PVA) and positive (PLGA/CS) NPs were prepared by dissolving 100 mg of PLGA (75:25 Resomer® RG756) Boehringer-Ingelheim (Ingelheim, Germany) in dichloromethane/acetone (1/1 v/v) mixture and pre-emulsifying by vortexing for 1 min with 20 mL of an aqueous solution of 2.5 mg mL^{-1} PVA (87–89% hydrolyzed, 30–70 kDa, Sigma Aldrich, Lyon, France) for PLGA/PVA or with 0.6 mg mL^{-1} chitosan (Protosan® UP CL113, 75%–90% deacetylation, 50–150 kDa, NovaMatrix®, FMC BioPolymer, Drammen, Norway) and 5 mg mL^{-1} PVA (Mowiol® 4-88 PVA, 30 kDa, a gift from, Kuraray Specialties Europe GmbH, Frankfurt, Germany) for PLGA/CS. The mixture was kept on ice and sonicated (Branson Digital Sonifier) at 80 W for 1 or 2 min, respectively. For the preparation of negatively charged (PLGA/PF68) NPs, 50 mg of PLGA were dissolved in 5 mL of ethyl acetate, this organic phase was added dropwise to 10 mL of a 10 mg mL^{-1} poloxamer 188 [Pluronic® F68 (PF68), BASF, Levallois Perret, France] aqueous solution under magnetic stirring. This mixture was then vortexed for 1 min and kept on ice during a 2 min homogenization at 10 000 rpm using an Ultra-Turrax (IKA®-Werke GmbH & Co. KG, Staufen, Germany) equipped with an 18G stainless steel dispersing tool. For all preparations, the organic phase was evaporated at room temperature overnight under magnetic stirring (600 rpm). The purification of PLGA/PVA and PLGA/CS (removal of stabilizers) NPs was done by ultracentrifugation at 37 000 × *g* for 1 h at 4 °C. Pellets were resuspended in MilliQ® water (Millipore, Molsheim, France) by vortexing. PLGA/PF68 NPs were purified by dialysis during 24 h against MilliQ® water using a cellulose ester membrane with a 50 kDa cut off (SpectrumLabs, Breda, The Netherlands). For *in vivo* imaging studies, PLGA NPs covalently labeled with DY-700, a near-infrared dye, were used (Reul et al., 2012). The same protocol was followed with the formulation reduced to one quarter (25 mg of PLGA in total) and by replacing 1% of PLGA RG756 by DY-700-PLGA conjugate (Reul et al., 2012). TiO_2 suspensions were prepared by dispersion of anatase (spheres, < 25 nm) or rutile (rods, 10 × 40 nm) TiO_2 nanopowders (Sigma-Aldrich, Lyon, France) in MilliQ® water. Briefly, a 1 mg mL^{-1} suspension of TiO_2 nanopowder was vortexed and had its pH adjusted to 11 with 1 M NaOH. Suspensions were sonicated at 40% on ice for 1.5 h (cycles of 60 s sonication and 30 s pause) and then homogenized at 24 000 rpm for 5 min on ice using an Ultra-Turrax disperser equipped with a plastic (polycarbonate/PEEK) dispersing tool (S25D-14G-KS, IKA, ®-Werke GmbH & Co. KG, Staufen, Germany). Polystyrene NPs (PS) are commercially available as an aqueous suspension of 0.20 µm NPs (PolySciences Europe GmbH, Eppelheim, Germany). All NPs were tested as endotoxin-free at the concentrations they were given to animals.

Nanoparticle characterization

Nanoparticle average diameter size and polydispersity index were determined after dilution in MilliQ® water at 25 °C by dynamic light scattering (DLS) using a Nano ZS (Malvern Instruments, Worcestershire, UK), with a 173 ° scattering angle. The zeta potential was determined using the same instrument after dilution in 1 mM NaCl. All measurements were done in triplicate.

The morphology of NPs in aqueous suspension was studied by transmission electron microscopy (TEM) using a JEOL JEM-1400 microscope operating at 80 kV (filament current of 55 µA). A 5 µL of NP aqueous suspensions was deposited onto copper grids covered with formvar film (400 mesh) for 1 min. PLGA samples were then stained using 2% phosphotungstic acid (PLGA/PVA, PLGA/PF68) or 2% uranyl acetate (PLGA/CS) for 30 s, while TiO_2 samples were used without staining. The excess liquid was blotted off using filter paper, and the grids were dried before observation. Images were acquired using a post-column high-resolution (11 megapixels) high-speed camera (SC1000 Orius; Gatan) and processed with Digital Micrograph (Gatan) and ImageJ (open source software, Research Services Branch, National Institute of Mental Health, Bethesda, MD).

Animals

Toxicity of NPs was investigated in Balb/cJ mice (4 weeks-old, $n = 4$–6/group) purchased from Janvier laboratories (France). Food and water were administered *ad libitum*. Mice were housed in plastic cages under controlled environmental conditions (temperature 19–21 °C, humidity 40–70%, lights on 07:00 h to 19:00 h). Mice were acclimated to these conditions for 7 days before experiments started. The rules from the local ethics committee (Comité d'éthique pour l'expérimentation animale, protocol number 2012-117) were followed.

Biodistribution of NPs was followed in NMRI nude mice (4 weeks old) purchased from Janvier laboratories (France). Mice were submitted to the above cited conditions in addition to being housed under germ-free environment.

Pulmonary delivery of aerosolized NPs

Nebulization was performed as previously described (Bivas-Benita et al., 2005) with some adaptations. Balb/c mice were exposed to 3% isoflurane (CSP, Cournon-d'Auvergne, France) and, once a deep stage of anesthesia was reached, mice were transferred to a mouse intubation platform and intratracheally nebulized by means of MicroSprayer® Aerozolizer system (MicroSprayer® Aerozolizer-Model IA-1C and FMJ-250 High Pressure Syringe, Penn Century, Wyndmoor, PA) with 50 µL of 5% glucose (vehicle) or with a suspension containing 250 µg of either PLGA/CS, PLGA/PVA, PLGA/PF68, PS, anatase TiO_2 or rutile TiO_2 NPs in 5% glucose (final pH 6–7). For the nebulization, mice were suspended by the upper teeth at a 45 ° angle, in supine position, on an intubation platform (Hallowell EMC, Pittsfield, MA). The mouth was opened, the tongue was displaced with the help of a forceps and a mouse intubation speculum (Hallowell EMC) attached to an otoscope (WelchAllyn Inc., Skaneateles Falls, NY) was inserted for oropharyngeal visualization. Once a clear view of the trachea was obtained, with the visualization of the vocal chords, the MicroSprayer tip was endotracheally inserted and 50 µL of the solution or suspensions were sprayed. The tip was withdrawn and the mouse was taken off the support and allowed to recover under visual control before being placed back in cage. One set of mice ($n = 4$–6/group) was euthanized 24 or 48 h following a single nebulization and the bronchoalveolar lavage fluid (BALF) was collected and analyzed for cellular and biochemical inflammatory markers. Another set of mice ($n = 4$–6/group) was used for lung excision and fixation for histological analysis 24 h after a single nebulization.

Before conducting the experiments, the efficacy of the nebulization procedure was evaluated by nebulizing mice with 50 µL of 4% Trypan blue solution. Animals were sacrificed immediately after nebulization and lung distribution was visualized in the dissected lung.

Bronchoalveolar lavage

BAL collection was adapted from previously described techniques (Maxeiner et al., 2007; Segel et al., 2005). Briefly, the trachea was surgically exposed and a small incision was made between tracheal rings to allow the insertion of a polyethylene tube attached to a 21 G syringe needle, which was secured with a suture thread. Lungs were instilled successively with isotonic ice-cold saline that

was gently retrieved. The first two lavages (300 and 400 µL) were collected in a 1.5 mL tube and the subsequent (500 µL, eight times) in a 15 mL tube, which rendered about 4 mL of bronchoalveolar lavage fluid (BALF). After centrifugation at 400 × *g* for 15 min at 4 °C, the supernatant from the first two lavages was stored at −20 °C for later biochemical analysis and the cell pellets were pooled and resuspended in 1 mL of saline for cell count in Neubauer chamber, using the Trypan Blue exclusion method.

BALF differential cell count and imaging

Differential cell count was performed after a cell aliquot from BALF (50 000 cells) was smeared in duplicate onto slides using Cytospin™ 4 cytocentrifuge (Thermo Scientific™, Saint Aubin, France) at 600 rpm for 10 min, with break, at room temperature. Cytoslides were fixed and thereafter stained with May–Grünwald–Giemsa prior to manual cell count using light microscopy to assess morphology of 400 cells per slide. Macrophages, neutrophils, eosinophils, basophils and lymphocytes were identified by their characteristic shapes. Light microscopic images of stained cells were taken with Leitz Diaplan microscope (Leica Microsystems Wetzlar GmbH, Wetzlar, Germany).

Total protein quantification

Total protein content in BALF was measured spectrophotometrically at 595 nm according to the Bradford method using bovine serum albumin as standard. Manufacturer's protocol for Bio-Rad Protein Assay (Bio-Rad Laboratories GmbH, Munich, Germany) performed on microtiter plate was followed and each sample was run in triplicate.

Cytokine measurements

Cell-free BALF was used for cytokine analysis using BD™ Cytometric Bead Array mouse inflammation kit (BD Biosciences, Le Pont de Claix, France) in which interleukin (IL)-6, IL-12p70, IL-10, tumor necrosis factor (TNF), interferon-γ (IFN-γ) and monocyte chemoattractant protein-1 (MCP-1), also referred to as chemokine (C–C motif) ligand 2 (CCL2), were measured. Samples were acquired on BD Accuri™ C6 flow cytometer (BD Biosciences, Le Pont de Claix, France) and analyzed with the FCAP Array™ software. The predicted assay detection limit is 5 pg mL^{-1} for IL-6, 17.5 mg mL^{-1} for IL-10, 52.7 mg mL^{-1} for MCP-1, 2.5 mg mL^{-1} for IFN-γ, 7.3 mg mL^{-1} for TNF and 10.7 mg mL^{-1} for IL-12p70.

Table 1. Average diameter, polydispersity index and zeta potential of nanoparticles.

Nanoparticle type	Diameter (nm)	PDI[a]	ζ-Potential (mV)
PLGA/PVA	223 ± 16	0.07 ± 0.03	−4.0 ± 1.2
PLGA/CS	204 ± 17	0.20 ± 0.02	+17.8 ± 4.2
PLGA/PF68	236 ± 12	0.12 ± 0.03	−34.6 ± 6.2
DY-700-PLGA/PVA	252 ± 5	0.14 ± 0.04	0.0 ± 1.3
DY-700-PLGA/CS	205 ± 10	0.17 ± 0.04	+22.8 ± 5.5
DY-700-PLGA/PF68	245 ± 44	0.13 ± 0.02	−29.3 ± 14
PS	230 ± 2.3	0.01 ± 0.01	−54.5 ± 0.5
Anatase TiO_2	412 ± 2.3	0.31 ± 0.02	−22.4 ± 1.9
Rutile TiO_2	398 ± 34	0.71 ± 0.06	−59.3 ± 2.1

[a]Polydispersity index. Data are presented as mean ± SD.

Histopathological evaluation

At 24 h after nebulization, lung tissue was dissected, rinsed from blood with PBS and fixed in phosphate-buffered 4% paraformaldehyde (Fisher Scientific, Illkirch, France) at 4 °C overnight. Paraffin-embedded lungs were 5 µm sectioned and stained with hematoxylin–eosin (H–E). Slices were evaluated by an anatomopathologist using light microscopy.

In vivo distribution of PLGA NPs

NMRI nude mice (6–8 weeks old, Janvier, France; $n = 2$–3/group) were anesthetized with a medetomidine (200 µg kg of BW^{-1}, Dormitor®, Orion Pharma, Espoo, Finland) and ketamine (100 mg.kg of BW^{-1}, Imalgéne, Merial, France) mixture in phosphate buffered saline and intratracheally nebulized by means of MicroSprayer® Aerozolizer system with 50 µL of a suspension of 250 µg of DY-700-PLGA-/CS, DY-700-PLGA/PVA or DY-700-PLGA/PF68. Mice were sacrificed by cardiac exanguination under anesthesia 1.5-2% mixture of isoflurane anesthesia (CSP, Cournon-d'Auvergne, France) at 2, 5, 8, 24 and 48 h after nebulization for visualizing the *ex vivo* fluorescence of tissues (stomach, lung, lymph node, brain, skin, muscle, kidney, adrenal, bladder, intestine, spleen, pancreas, fat and liver) and plasma. Tissues were illuminated by 675 mm light-emitting diodes equipped with interference filters and emission was collected by 720/20 nm pass-band filter (IVIS Kinetic, Caliper Life Sciences Inc., Hopkinton, MA). Fluorescence images were acquired during 10 s and image analysis was performed using the Wasabi software (Hamamastsu, Massy, France). Semi-quantitative data were obtained by drawing regions of interest (ROI) around each organ. Fluorescent images were acquired by a back-thinned CCD camera at −80 °C (ORCAII-BT-512 G, Hamamatsu, Massy, France).

Statistical analysis

Statistical differences were tested by one-way analysis of variance (ANOVA) followed by the Dunnett *post-hoc* test. Two-way ANOVA was applied for tissue fluorescence data, followed by the Bonferroni *post-hoc* test. For cytokine measurements, the concentration in samples below the detection limit was set to 0. Data analysis was considered significant at $p < 0.05$ or lower.

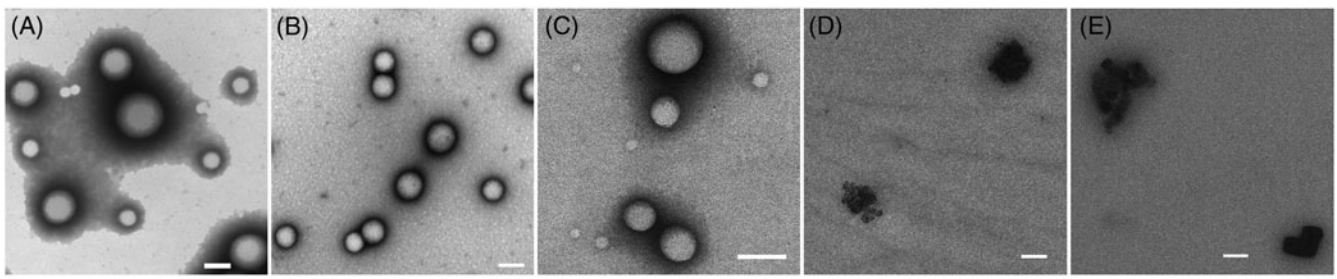

Figure 1. NP morphology as observed by transmission electron microscopy of aqueous suspensions of (A) PLGA/PVA, (B) PLGA/CS, (C) PLGA/PF68, (D) anatase TiO_2 and (E) rutile TiO_2; bar = 100 nm (A, B, C) or 200 nm (D, E).

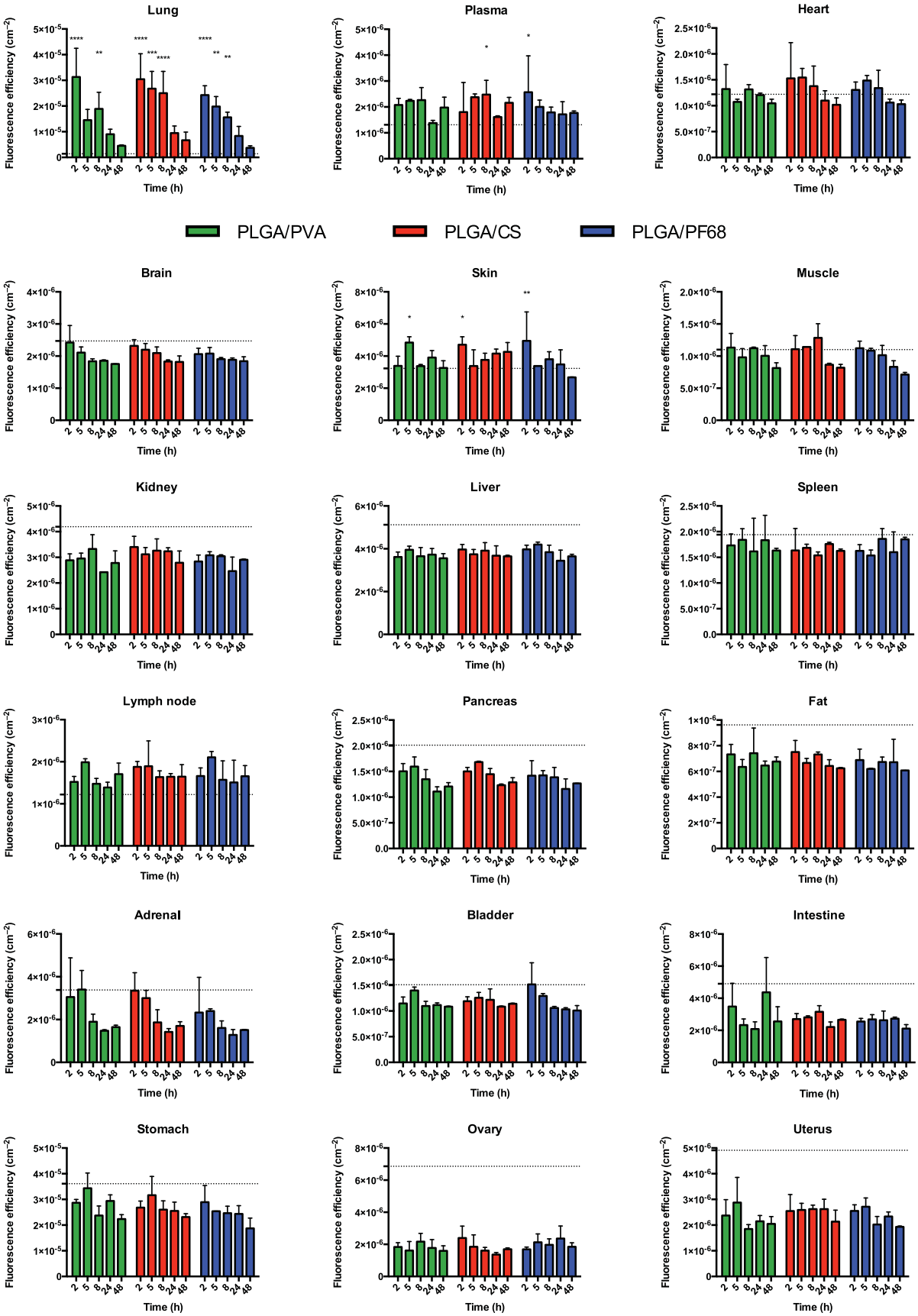

Figure 2. NP biodistribution. Fluorescence efficiency was detected in various tissues of NMRI nude mice at 2, 5, 8, 24 or 48 h after single nebulization with either DY-700-PLGA/PVA, DY-700-PLGA/CS or DY-700-PLGA/PF68. Reference (dotted) line shows the autofluorescence levels measured in untreated animals.

Results

Nanoparticle characterization and administration

The established protocol for preparing PLGA NPs using different stabilizers produces NPs with different surface charges. All PLGA NPs displayed a similar mean hydrodynamic diameter, from 200 to 250 nm (Table 1). The size distributions of PLGA NPs were very narrow, as indicated by their low polydispersity indices (0.1–0.2). Zeta potential measurements illustrate the influence of the stabilizers on the surface charge, in which PLGA/PVA NPs exhibited a close to neutral zeta potential (-4.0 ± 1.2 mV), PLGA/CS had a positive surface charge ($+17.8 \pm 4.2$ mV) and PLGA/PF68 had a negative surface charge (-34.6 ± 6.2 mV). All PLGA-based NPs exhibited a spherical shape as observed by TEM (Figure 1). The presence of fluorescent DY-700-PLGA did not alter PLGA NP characteristics (Table 1). Commercially available PS NPs show a similar mean diameter (230 ± 2.3 nm) as PLGA NPs and display a negative zeta potential (-54.5 ± 0.5 mV; Table 1). The suspension of TiO_2 nanopowders (50 nm anatase TiO_2 spheres and rutile TiO_2 rods) in water resulted in aggregates exhibiting a mean diameter around 400 nm, a zeta potential of -22.4 ± 1.9 mV and -59.3 ± 2.1 mV, respectively (Table 1), without any specific sphere/rod pattern. Mice were exposed to NPs with an aerosolizer delivery system that allows for a better lung distribution. The validation of the intratracheal nebulization was done by administering Trypan blue solution. Bilateral staining was observed in the lungs of mice (data not shown).

Biodistribution and elimination of PLGA NPs

In order to investigate the *in vivo* distribution and the persistence of PLGA NPs, mice were exposed to a single intratracheal nebulization with each of the three kinds of DY-700-PLGA NPs and tissue fluorescence was detected at post-nebulization time points 2, 5, 8, 24 and 48 h. The distribution profile of PLGA NPs in organs following nebulization is shown in Figure 2. A high fluorescence signal came from the stomach, but was attributed to autofluorescence from food and was not correlated to time or treatments. An important fluorescence signal was observed in the lungs 2 h after nebulization and gradually decreased over time, with a pattern that was similar among all DY-700-PLGA NPs regardless of their surface charge. The fluorescence decrease fitted to an exponential decay, with a similar elimination constant among PLGA NPS (0.05–0.40 h^{-1}, corresponding to a half life between 17.5 and 19.9 h) (Figure 3). Very low fluorescence was observed in the plasma, in which only two fluorescence values were significantly higher than the basal level (PLGA/CS after 8 h; PLGA/PF68 after 2 h). A few significant fluorescence increases were noted for the skin compared to the basal level. No other significant increase was noted in all other investigated organs and tissues: heart, brain, muscle, kidney, liver, spleen, lymph nodes, pancreas, fat, adrenal, bladder and intestine (Figure 2).

Inflammatory response to NPs

Cellular content of BAL

We have investigated the pulmonary inflammatory response to determine the impact of exposing mice to a single intratracheal nebulization of PLGA NPs (polymeric, biodegradable), PS (polymeric, non-biodegradable) and TiO_2 NPs (inorganic, non-biodegradable). The recruitment of inflammatory cells into the lung lumen was assessed. The total number of BAL cells and the number of macrophages, neutrophils, lymphocytes and eosinophils in BAL cells (Figure 4A–E) were determined. The exposure to the different polymeric NPs did not result in changes in the total number of cells recovered from BAL, as was true for rutile

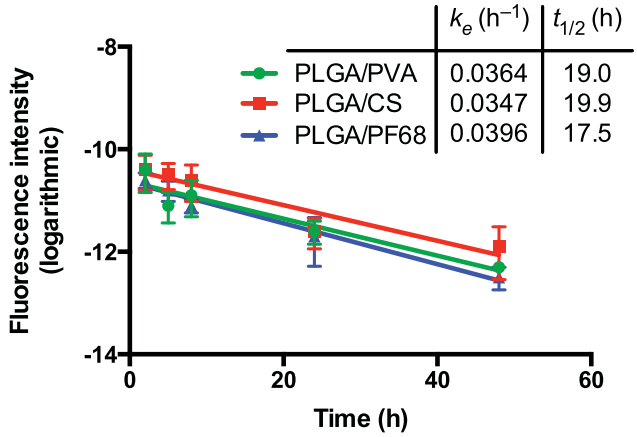

Figure 3. Lung elimination half-lives for PLGA/PVA, PLGA/CS, PLGA/PF68 in NMRI nude mice after single nebulization with either DY-700-PLGA/PVA, DY-700-PLGA/CS or DY-700-PLGA/PF68.

TiO_2 NPs (Figure 4A). However, a significantly higher number of cells was observed for anatase TiO_2 exposed mice at 24 h after nebulization; this increase was transitory as total cell count returned to levels that were similar to the control group at 48 h.

Macrophage is the predominant cell population in the BAL from healthy animals (Figure 4C). 24 and 48 h after nebulization, the BAL from mice exposed to biodegradable PLGA and PS NPs showed a slight variation in the number of macrophages that remained in levels that were similar to control groups (Figure 4B). At 24 h, the number of macrophages was not changed in anatase TiO_2 group (levels decreased 48 h after nebulization), while mice exposed to rutile TiO_2 had a significant increase in the number of macrophages in BAL. In parallel, a recruitment of neutrophils was noted 24 h after nebulization in PS and anatase TiO_2 exposed mice, which was significant in the anatase TiO_2 group (Figure 4C). The recruitment of neutrophils persisted in the same groups after 48 h, but showed a tendency for reduction. The number of lymphocytes and eosinophils accounted for less than 1% of total BAL cells in all groups and no significant difference was observed among groups (Figure 4D and E).

Internalization of NPs by lung cells

The internalization of particles was observed in cytospun lung cells visualized under light microscopy and, for all polymeric NPs, a tendency to an increase in macrophages cytoplasm volume and an accumulation of aggregates in the cytoplasm of some cells could be noted, both at 24 and at 48 h after nebulization (Figure 4F). The accumulation of rutile and anatase TiO_2 NPs was well visible as high contrast aggregates in the cytoplasm of lung cells at both time points.

BALF protein quantification

The amount of proteins in the BALF is usually a prediction for inflammatory response. The protein quantification revealed no significant changes in all groups of NP-exposed mice (Figure 5), but PS and anatase TiO_2 groups showed a trend to mirror the results obtained for neutrophil recruitment, even if the increase in protein quantification observed for these groups did not hit statistical significance.

Cytokines in BALF

An early and transient increase of IL-6, MCP-1 was detected in the BALF of PS exposed mice (Figure 6), the same pattern could be seen for TNF, but did not reach significant difference. In BALF

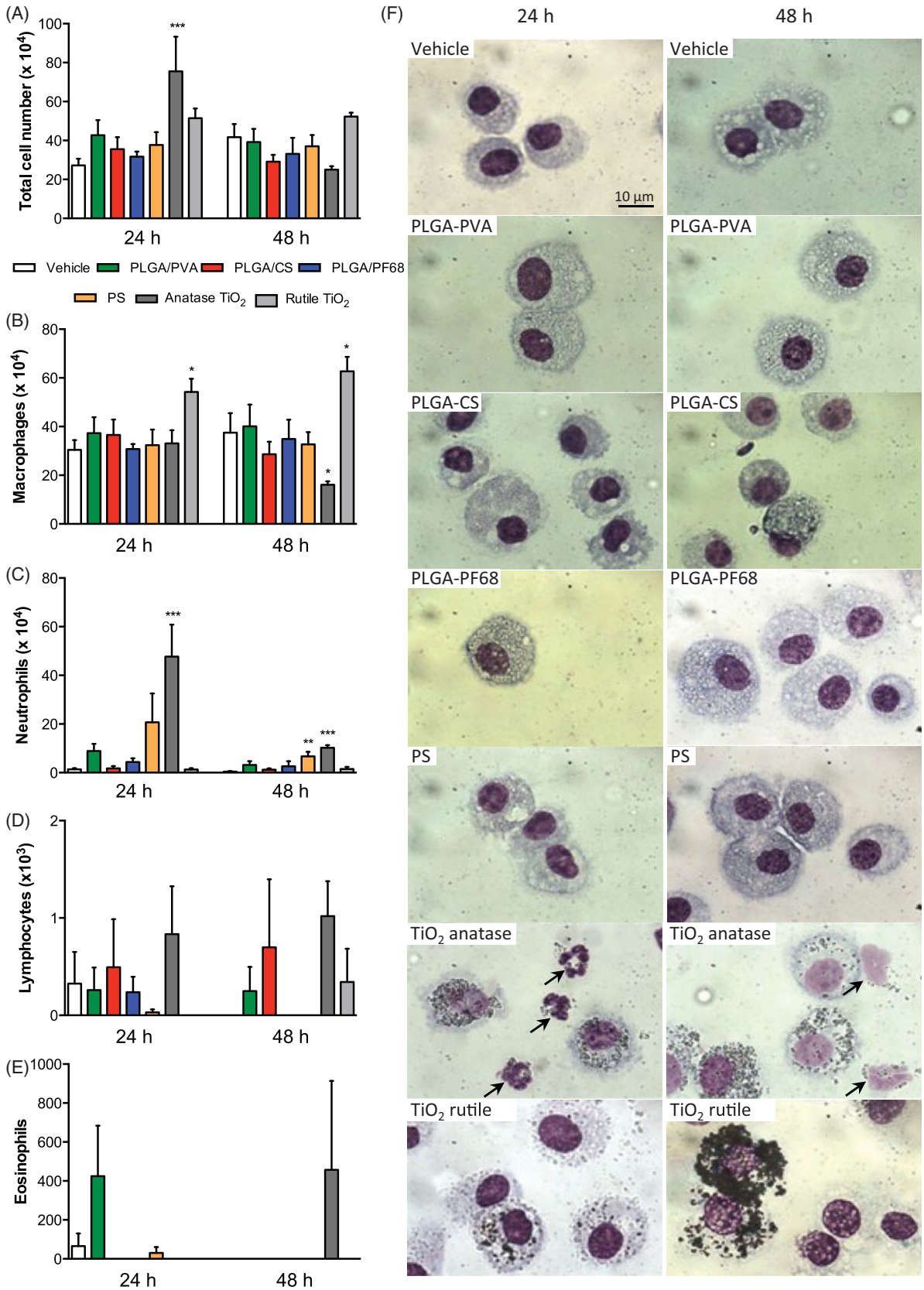

Figure 4. Assessment of BAL cells from Balb/cJ mice 24 or 48 h after single intratracheal nebulization of vehicle or PLGA/PVA, PLGA/CS, PLGA/PF68, PS, TiO_2 anatase and TiO_2 rutile NPs. Total BAL cell population number (A). Differential cell count in May–Grünwald–Giemsa stained BAL cells allowed identification of macrophages (B), neutrophils (C), lymphocytes (D) and eosinophils (E). Light microscopic images show particle internalization by lung cells, mostly macrophages, collected 24 (left panel) or 48 h (right panel) after mice were intratracheally nebulized (F). Arrows show neutrophils. Original magnification 1000-fold (Leitz Diaplan). $*p<0.05$, $**p<0.05$, $***p<0.001$ versus vehicle (ANOVA with Dunnett *post-hoc* comparison).

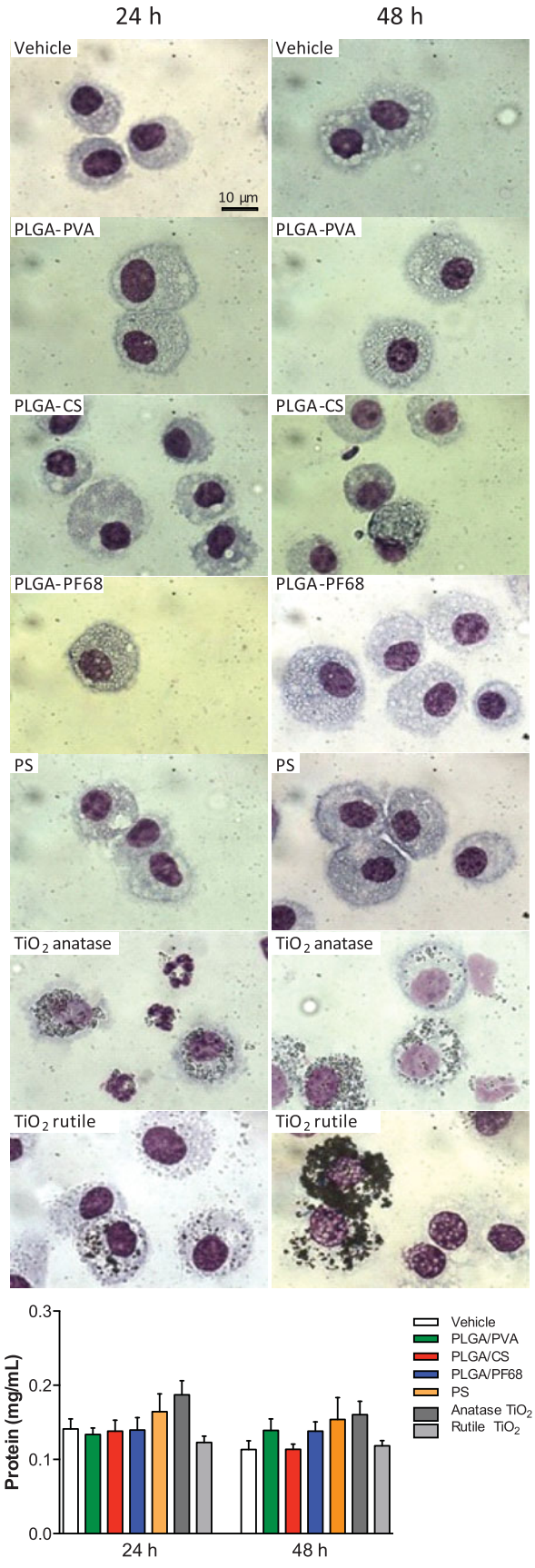

Figure 5. Effect of NPs on total protein content in BALF. Balb/cJ mice were exposed to a single intratracheal nebulization with NPs and BAL was collected after 24 or 48 h. Total protein was quantified by the Bradford method. Data represent mean ± standard error of the mean (SEM).

from anatase TiO_2-exposed mice, an increase of IL-6 and MCP-1 was observed at both time points, reaching significant increase at 48 h. TNF levels were increased at 24 h in the anatase TiO_2 group, this effect persisted at 48 h. Most groups had undetectable levels of both IFNγ and IL-12p70, the exception being anatase TiO_2-exposed mice in which this cytokine was detected at a low level. Small variations in cytokine levels were observed for PLGA NPs, but mostly not significantly different from control groups.

Histology

Anatomo-pathological examination of lung tissue sections 24 h after nebulization of NPs revealed no or mild changes in tissue from PLGA NP-exposed mice compared to the control group, with a loose structure and mild neutrophilic infiltration (Figure 7). In mice exposed to PS and especially anatase or rutile TiO_2 NPs, a thickening of interstitial wall was observed as well as erythrocyte accumulation. TiO_2 NP uptake was observed by accumulation of aggregates inside lung macrophages and interstitial space (Figure 7).

Discussion

In this study, the influence of surface charge on the biodistribution of biodegradable PLGA NPs was investigated after intratracheal nebulization in mice, as well as their lung toxicity, through their inflammatory potential, in comparison with non-biodegradable NPs, either polymeric (PS) or inorganic (rutile and anatase TiO_2). By means of addition of three different stabilizing agents, CS, PVA or PF68, we have obtained PLGA NPs with a diameter of around 220 nm that displayed a positive, neutral or negative surface charge, respectively.

Previous *in vitro* results from our group indicated that the internalization of PLGA NPs could vary depending on their surface charge and on the cell type. For A549 cells, a model of alveolar epithelium, a higher internalization of PLGA/PF68 NPs was seen in comparison with PLGA/CS and PLGA/PVA, and an association of PLGA/CS with the cell membrane was also evident (Grabowski et al., 2013). On the other hand, for Calu-3 cells, a bronchial epithelium model, no changes were observed for the internalization of NPs, but surface charge exerted influence in the transport across the mucus layer and negatively charged PLGA/PF68 NPs passed by the mucus layer more easily, reaching the cells more rapidly than PLGA/CS and PLGA/PVA (Mura et al., 2011a,b). In this study, the biodistribution of fluorescent PLGA NPs was followed in various time points until 48 h after intratracheal nebulization. Lung retention was evidenced by an initial increase in fluorescence 2 h after nebulization and a gradual elimination. The lung elimination half-time for these biodegradable PLGA NPs was similar and, in contrast with previous *in vitro* results, their surface charge had little influence over their accumulation and elimination from mice lungs.

The biodistribution of PS and TiO_2 NPs could not be traced in our study due to the unavailability of a fluorescent form of these NPs. However, we could assume that the 230 nm PS NPs used in this study show a similar distribution pattern to what has been described for 250 nm PS NPs from the same manufacturer. A short time monitoring (5 h) after intratracheal instillation in BALB/c mice showed a quick initial clearance of PS NPs from lung and migration to other tissues, with an accumulation in lymph nodes (Mohammad et al., 2013).

Indirect measurements of PLGA NPs distribution after intratracheal instillation using FITC encapsulated in negatively charged PLGA NPs showed a quick passage through the lung with detection of FITC staining in the liver and kidney after only 15 min (Hara et al., 2008). However, the authors do not rule out

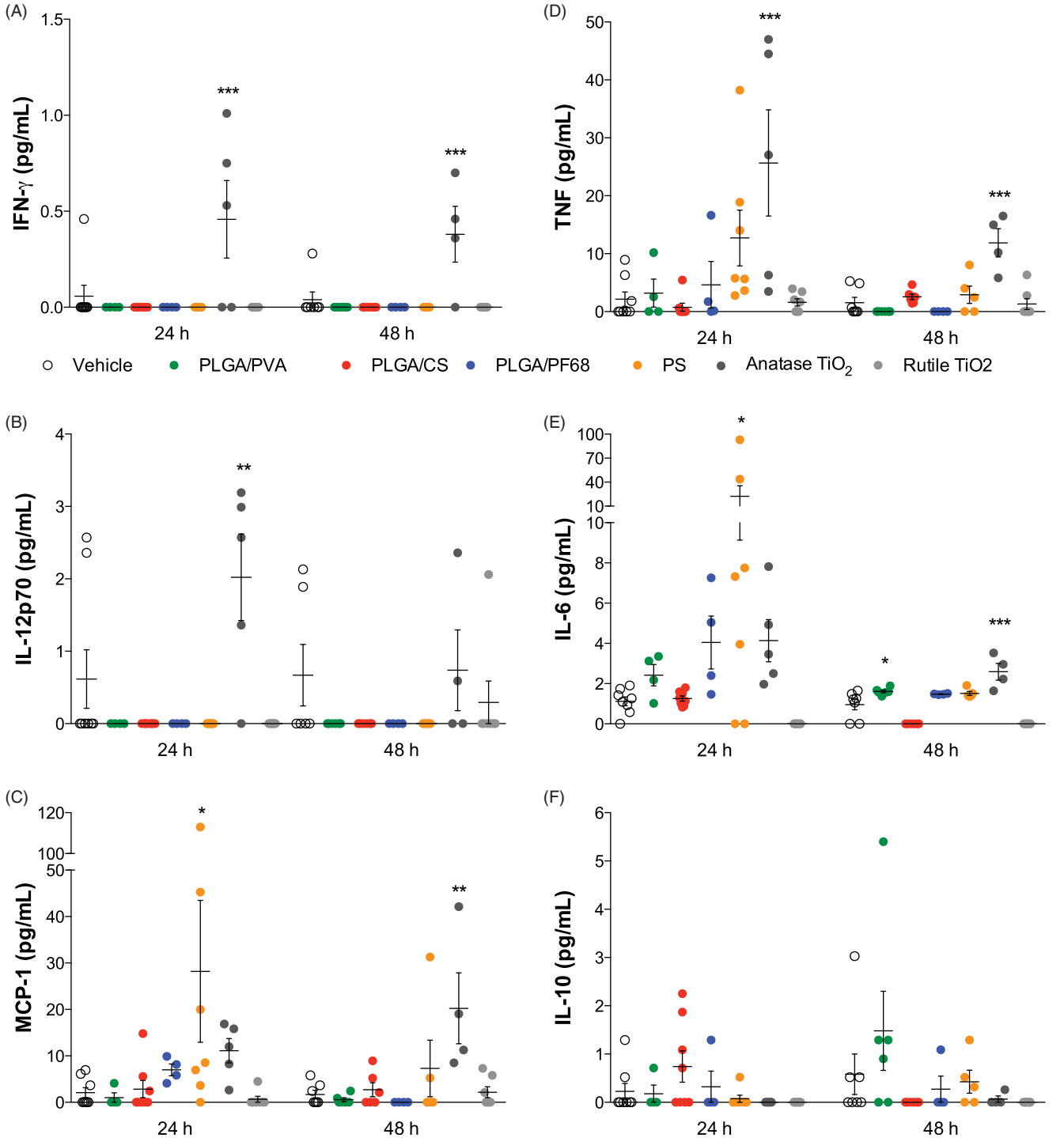

Figure 6. Effect of NPs on cytokine release in BALF from Balb/cJ mice. Concentration of (A) IL-6, (B) TNF, (C) MCP-1, (D) IL-10, (E) IFN-γ and (F) IL-12p70 in cell-free BAL collected 24 or 48 h after single lung nebulization with NPs. *$p < 0.05$, **$p < 0.05$, ***$p < 0.001$ versus vehicle (ANOVA with Dunnett *post-hoc* comparison).

the possibility of the staining being a result of the passage of free FITC and not NP encapsulated FITC. In our study, DY-700 is covalently bound to PLGA, which makes it more likely that the observed fluorescence does not come from the free DY-700, but from either DY-700-PLGA NPs or from DY-700-PLGA conjugate. Given the common characteristics between PLGA NPs and PS NPs, such as smooth surface morphology and monodispersity, it could be postulated that PLGA would have a similar biodistribution. Despite these similarities, we saw little migration to other tissues and no accumulation of PLGA NPs in the mesenteric lymph node. Although no difference in biodistribution was observed among our PLGA NPs, surface charge could play a role in the site of lung deposition of PLGA NPs. Positively charged porous PLGA NPs have been shown to deposit earlier in the respiratory tract, being located in trachea, bronchia and bronchioles, whereas negatively porous charged PLGA NPs reached further and were mainly located in alveolar ducts (Ungaro et al., 2012).

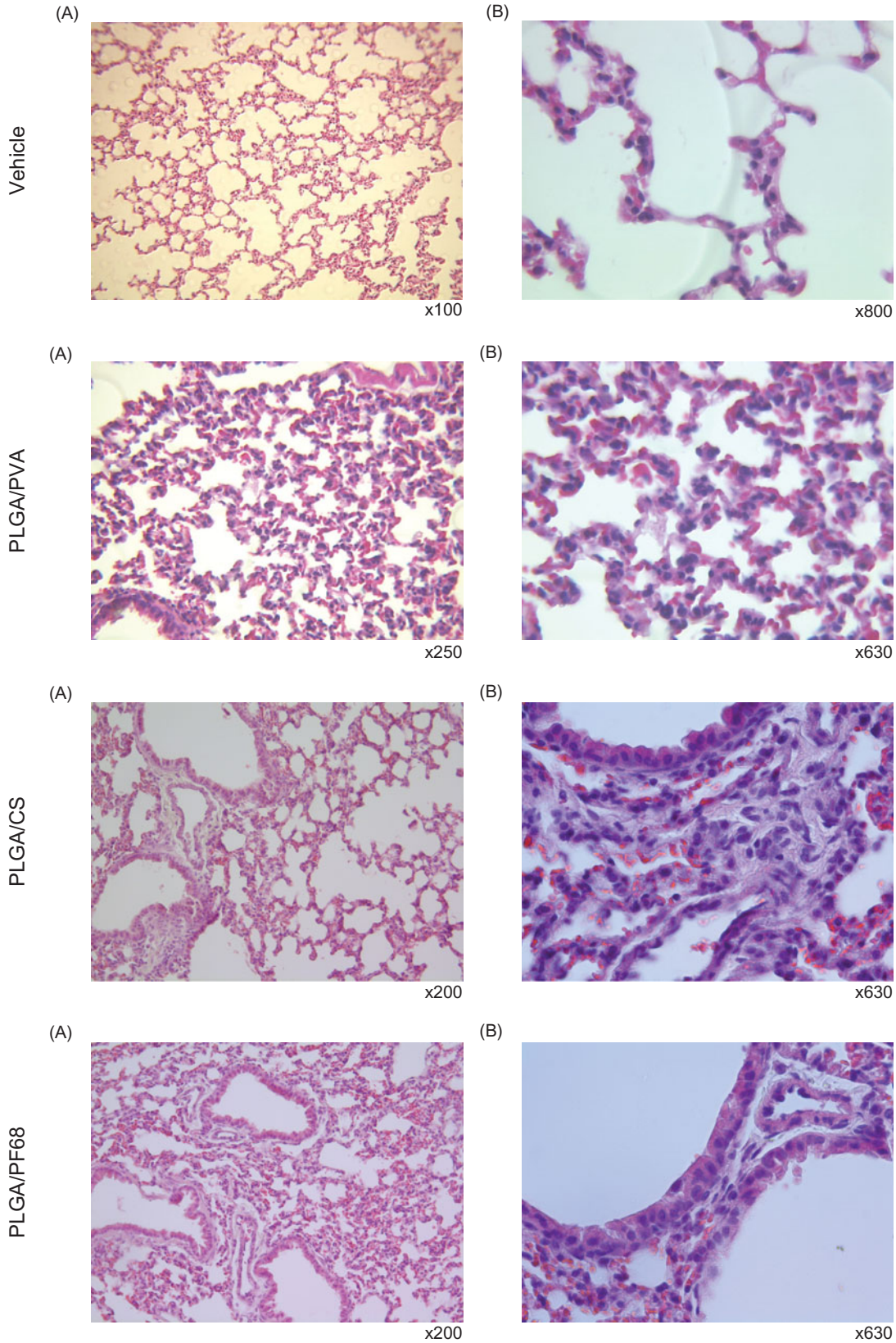

Figure 7. Histological observations at low (A) and high (B) magnification of lung tissue of Balb/cJ mice 24 h after intratracheal nebulization of vehicle or PLGA/PVA, PLGA/CS, PLGA/PF68, PS, TiO_2 anatase and TiO_2 rutile NPs. Arrows show erythrocyte accumulation.

With regards to the distribution of TiO_2 NPs, we could expect a long permanence of these NPs in the lungs of mice, since a very long biological half-time of 10.8 months was observed in rats receiving a single intratracheal instillation of 21 nm TiO_2 NPs at a similar dose to that of our study (Oyabu et al., 2013). Also, a long biological half-time was observed after chronic inhalation of 21 nm TiO_2 NPs by mice (Bermudez et al., 2004).

No significant change in the amount of proteins from BALF was detected for all NPs studied, contrasting with previous reports in which PS NPs induced a transient increase in protein concentration (Dailey et al., 2006). Similarly though, mice

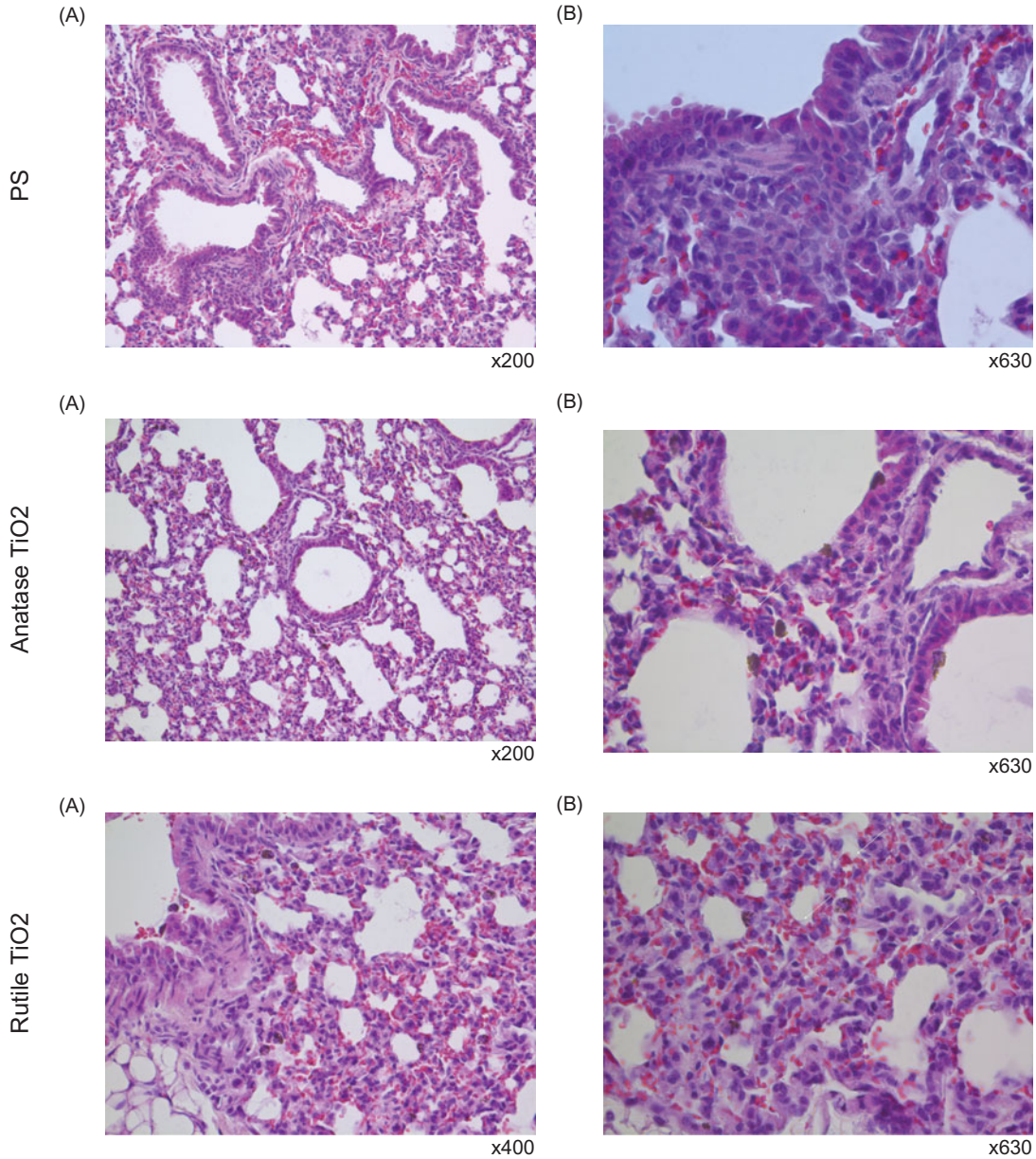

Figure 7. Continued.

exposure to PS NPs caused an increase in the recruitment of neutrophils that was subsequently reduced after 48 h. Despite the non-biodegradability of PS NPs, the lower inflammatory response in comparison to anatase TiO_2 could be due to faster lung elimination and to the translocation of PS NPs to other organs (Mohammad et al., 2013).

Lung exposure to anatase TiO_2 NPs elicited a transitory increase in neutrophil count and triggered the innate immune response illustrated by an increase in the levels of TNF-α, IL-6, MCP-1, IFNγ and IL-12p70 cytokines, which are typical of the classically activated macrophage (Gally et al., 2011). This response has been described previously for TiO_2 NPs exposure which induced the expression of markers of inflammation, the recruitment of neutrophils and lead to accumulation of macrophages containing NPs in the lung tissues, even then not resulting in emphysematous or fibrotic changes (Driscoll & Maurer, 1991; Saber et al., 2012). Moreover, the expression of genes involved in ion homeostasis and muscle function were altered after exposure to TiO_2, which could possibly lead to the development of lung diseases (Husain et al., 2013).

A distinct inflammatory potential was noted between anatase TiO_2 and rutile TiO_2, in which the latter did not induce an inflammatory response. These results could be attributed to a higher membrane damage induced by the crystal structure of anatase TiO_2 (Braydich-Stolle et al., 2009), which can be correlated with a decrease in macrophage count after 48 h. The production of ROS was increased after exposure of cultured keratinocytes to rutile TiO_2, but was controlled with addition of antioxidant to the culture media (Braydich-Stolle et al., 2009). In lung cells, ROS production induced by rutile TiO_2 NP might be balanced by the intrinsic antioxidative capacity of these cells, resulting in a low toxic response.

Low toxicity has been reported after lung exposure to uncoated 83 nm PLGA NPs where no alterations were found for lactate dehydrogenase (LDH) release, protein quantity, expression of macrophage inflammatory protein-2 (MIP-2) or neutrophil recruitment in BAL (Dailey et al., 2006). Here, we showed that lung exposure to 200–250 nm PLGA NPs of neutral, positive or negative surface charge did not induce an inflammatory response

in mice, with no alterations of cellular population, protein quantity or expression of cytokines in BAL.

Conclusion

The results presented here indicate a safe use of biodegradable PLGA NPs for lung drug delivery. PLGA NPs of different surface charges showed low lung inflammatory potential evidenced by a reduced number of recruited neutrophils to lungs, low levels of cytokine release and of total protein in BALF.

Acknowledgements

The authors warmly thank Dr Dominique Berrebi, Françoise Gaudin-Nomé and Patrice Hémon (Histology platform, Inserm UMR 996, Clamart, France) for histological observations and help in interpretation and Sylvie Chollet-Martin (Inserm UMR 996) for helpful discussions. This work has used the facilities and the expertises of the Electron Microscopy Platform of the Imagif Cell Biology unit (Centre de Recherche de Gif – www.imagif.cnrs.fr) with the technical assistance of C. Boulogne.

Declaration of interest

The authors report no conflicts of interest. The authors alone are responsible for the content and writing of the paper. Institut Galien Paris-Sud is a member of the Laboratory of Excellence LERMIT supported by a grant from ANR (ANR-10-LABX-33). This study was supported by the Agence Nationale de la Recherche (under reference 2009 CESA 011) and by the Fonds de Dotation Recherche en Santé Respiratoire (appel d'offre 2011).

References

Bermudez E, Mangum JB, Wong BA, Asgharian B, Hext PM, Warheit DB, Everitt JI. 2004. Pulmonary responses of mice, rats, and hamsters to subchronic inhalation of ultrafine titanium dioxide particles. Toxicol Sci 77:347–57.

Bivas-Benita M, Zwier R, Junginger HE, Borchard G. 2005. Non-invasive pulmonary aerosol delivery in mice by the endotracheal route. Eur J Pharm Biopharm 61:214–18.

Braydich-Stolle LK, Schaeublin NM, Murdock RC, Jiang J, Biswas P, Schlager JJ, Hussain SM. 2009. Crystal structure mediates mode of cell death in TiO2 nanotoxicity. J Nanopart Res 11:1361–74.

Dailey LA, Jekel N, Fink L, Gessler T, Schmehl T, Wittmar M, et al. 2006. Investigation of the proinflammatory potential of biodegradable nanoparticle drug delivery systems in the lung. Toxicol Appl Pharmacol 215:100–8.

Driscoll KE, Maurer JK. 1991. Cytokine and growth factor release by alveolar macrophages: potential biomarkers of pulmonary toxicity. Toxicol Pathol 19:398–405.

Fattal E, Tsapis N. 2014. Nanomedicine technology: current achievements and new trends. Clin Transl Imaging 2:77–87.

Gally F, Di YP, Smith SK, Minor MN, Liu Y, Bratton DL, et al. 2011. SPLUNC1 promotes lung innate defense against mycoplasma pneumoniae infection in mice. Am J Pathol 178:2159–67.

Grabowski N, Hillaireau H, Vergnaud J, Santiago LA, Kerdine-Romer S, Pallardy M, et al. 2013. Toxicity of surface-modified PLGA nanoparticles toward lung alveolar epithelial cells. Int J Pharm 454: 686–94.

Grabowski N, Hillaireau H, Vergnaud-Gauduchon J, Nicolas V, Tsapis N, Kerdine-Römer S, Fattal E. 2016. Surface-modified biodegradable nanoparticles impact on cytotoxicity and inflammation response on a co-culture of lung epithelial cells and human-like macrophages. J Biomed Nanotechnol 12:135–46.

Hara K, Tsujimoto H, Tsukada Y, Huang CC, Kawashima Y, Tsutsumi M. 2008. Histological examination of PLGA nanospheres for intratracheal drug administration. Int J Pharm 356:267–73.

Husain M, Saber AT, Guo C, Jacobsen NR, Jensen KA, Yauk CL, et al. 2013. Pulmonary instillation of low doses of titanium dioxide nanoparticles in mice leads to particle retention and gene expression changes in the absence of inflammation. Toxicol Appl Pharm 269: 250–62.

Mansour HM, Rhee YS, Wu X. 2009. Nanomedicine in pulmonary delivery. Int J Nanomedicine 4:299–319.

Maxeiner JH, Karwot R, Hausding M, Sauer KA, Scholtes P, Finotto S. 2007. A method to enable the investigation of murine bronchial immune cells, their cytokines and mediators. Nat Protoc 2:105–12.

Mohammad A, Amayreh L, Mazzara J, Reineke J. 2013. Rapid lymph accumulation of polystyrene nanoparticles following pulmonary administration. Pharm Res 30:424–34.

Mura S, Hillaireau H, Nicolas J, Kerdine-Romer S, Le Droumaguet B, Delomenie C, et al. 2011a. Biodegradable nanoparticles meet the bronchial airway barrier: how surface properties affect their interaction with mucus and epithelial cells. Biomacromolecules 12:4136–43.

Mura S, Hillaireau H, Nicolas J, Le Droumaguet B, Gueutin C, Zanna S, et al. 2011b. Influence of surface charge on the potential toxicity of PLGA nanoparticles towards Calu-3 cells. Int J Nanomed 6:2591–605.

Oberdorster G, Oberdorster E, Oberdorster J. 2005. Nanotoxicology: an emerging discipline evolving from studies of ultrafine particles. Environ Health Perspect 113:823–39.

Oyabu T, Morimoto Y, Hirohashi M, Horie M, Kambara T, Lee B, et al. 2013. Dose-dependent pulmonary response of well-dispersed titanium dioxide nanoparticles following intratracheal instillation. J Nanopart Res 15:1–11.

Panyam J, Labhasetwar V. 2003. Biodegradable nanoparticles for drug and gene delivery to cells and tissue. Adv Drug Deliv Rev 55:329–47.

Reul R, Tsapis N, Hillaireau H, Sancey L, Mura S, Recher M, et al. 2012. Near infrared labeling of PLGA for in vivo imaging of nanoparticles. Polym Chem 3:694–702.

Saber AT, Jacobsen NR, Mortensen A, Szarek J, Jackson P, Madsen AM, et al. 2012. Nanotitanium dioxide toxicity in mouse lung is reduced in sanding dust from paint. Part Fibre Toxicol 9:4.

Segel MJ, Aqeilan R, Zilka K, Lorberboum-Galski H, Wallach-Dayan SB, Conner MW, et al. 2005. Effect of IL-2-Bax, a novel interleukin-2-receptor-targeted chimeric protein, on bleomycin lung injury. Int J Exp Pathol 86:279–88.

Singh RP, Ramarao P. 2013. Accumulated polymer degradation products as effector molecules in cytotoxicity of polymeric nanoparticles. Toxicol Sci 136:131–43.

Ungaro F, d'Angelo I, Coletta C, d'Emmanuele di Villa Bianca R, Sorrentino R, Perfetto B, et al. 2012. Dry powders based on PLGA nanoparticles for pulmonary delivery of antibiotics: modulation of encapsulation efficiency, release rate and lung deposition pattern by hydrophilic polymers. J Control Release 157:149–59.